J. Fluid Mech. (1994), *vol.* 279, *pp.* 49–68

Parametric instability of the interface between two fluids

By KRISHNA KUMAR AND LAURETTE S. TUCKERMAN†

Laboratoire de Physique, Ecole Normale Supérieure de Lyon, 46 allée d'Italie, 69364 Lyon Cedex 07, France

(Received 1 April 1993 and in revised form 25 April 1994)

The flat interface between two fluids in a vertically vibrating vessel may be parametrically excited, leading to the generation of standing waves. The equations constituting the stability problem for the interface of two viscous fluids subjected to sinusoidal forcing are derived and a Floquet analysis is presented. The hydrodynamic system in the presence of viscosity cannot be reduced to a system of Mathieu equations with linear damping. For a given driving frequency, the instability occurs only for certain combinations of the wavelength and driving amplitude, leading to tongue-like stability zones. The viscosity has a qualitative effect on the wavelength at onset: at small viscosities, the wavelength decreases with increasing viscosity, while it increases for higher viscosities. The stability threshold is in good agreement with experimental results. Based on the analysis, a method for the measurement of the interfacial tension, and the sum of densities and dynamic viscosities of two phases of a fluid near the liquid–vapour critical point is proposed.

1. Introduction

The generation of standing waves at the free surface of a fluid under vertical vibration has been known since the observations of Faraday (1831) (for a review see Miles & Henderson 1990). In a recent experiment by Fauve *et al.* (1992) with a closed vessel of liquid surrounded by its vapour under vertical oscillation, new phenomena were observed very close to the liquid–vapour (L–V) critical point. First, the wavelength saturates at a finite value as a function of frequency, and, second, the selected wave pattern at the onset consists of lines rather than the squares observed in previous experiments with low-viscosity fluids in contact with air at atmospheric pressure (see, for example, Ezerskii, Korotin & Rabinovich 1985; Tufillaro, Ramashankar & Gollub 1989; Ciliberto, Douady & Fauve 1991). As the temperature of the vessel is brought towards the L–V critical point, the difference in densities of the two phases and the surface tension of the interface decrease rapidly, while the viscosity of the two phases remains at some finite value. Consequently the wavelength decreases and the dissipation due to viscosity can no longer be treated as a small correction. One-dimensional standing waves (i.e. lines) are also observed at the free surface of a viscous glycerine–water mixture (Edwards & Fauve 1992) undergoing vertical oscillation. This further suggests the importance of viscosity.

Benjamin & Ursell (1954) studied the stability of the free surface of an ideal fluid theoretically and showed that the relevant equations are equivalent to a system of Mathieu equations. The dispersion relation in the ideal fluid case was in agreement

† Permanent address: Department of Mathematics and Center for Nonlinear Dynamics, University of Texas at Austin, Austin, TX 78712, USA.

with that found in low-viscosity fluid experiments. They estimated the viscous dissipation by treating it as a small perturbation but noted that the experimentally measured energy dissipation is actually much larger than this estimate. The prediction of the dispersion relation for two ideal fluids (see §4), however, does not agree with the experimental results of Fauve *et al.* (1992) close to the L–V critical point, and the estimated stability threshold based on a similar perturbative approach completely disagrees with the experimental one. In the light of these discrepancies, a linear stability analysis of the viscous problem seems necessary in order to understand the role of viscosity.

In this article we present a linear stability analysis of the interface between two viscous fluids. Starting from the Navier–Stokes equations, we derive the relevant equations describing the hydrodynamic system in the presence of parametric forcing and carry out a Floquet analysis to solve the stability problem. The viscous problem does not reduce to a system of Mathieu equations with a linear damping term, which is traditionally considered to represent the effect of viscosity. The traditional approach ignores the viscous boundary conditions at the interface of two fluids. To determine the effect of neglecting these, we compare our exact viscous fluid results with those derived from the traditional phenomenological approach. We also present the relevant equations governing the stability of a multilayer system of heterogeneous fluids (Appendix A) under parametric forcing. We propose a simple method for measuring the interfacial tension as well as the sum of densities and dynamic viscosities of two phases of a fluid near the L–V critical point.

2. Description of the hydrodynamical system

2.1. *Governing equations*

We consider two layers of immiscible and incompressible fluids, the lighter one of uniform density ρ_2 and viscosity η_2 superposed over the heavier one of uniform density ρ_1 and viscosity η_1, enclosed between two horizontal plates and subjected to a vertical sinusoidal oscillation. In a frame of reference which moves with the oscillating container, the interface between the two fluids is flat and stationary for small forcing amplitude, and the oscillation is equivalent to a temporally modulated gravitational acceleration. The equations of motion in the bulk of each fluid layer are:

$$\rho_j[\partial_t + (\boldsymbol{U}_j \cdot \boldsymbol{\nabla})]\,\boldsymbol{U}_j = -\boldsymbol{\nabla}(P_j) + \eta_j \nabla^2 \boldsymbol{U}_j - \rho_j G(t)\,\boldsymbol{e}_z, \tag{2.1}$$

$$\boldsymbol{\nabla} \cdot \boldsymbol{U}_j = 0, \tag{2.2}$$

where $j = 1, 2$ labels respectively the lower and the upper layer of fluids. The modulated gravitational acceleration is given by

$$G(t) = g - f(t) = g - a\cos(\omega t) \tag{2.3}$$

and can be compensated for by a pressure field. Linearizing about the state of rest $\boldsymbol{U}_j = 0$, $P_j(t) = -\rho_j G(t) z$, the equations for the perturbation fields $\boldsymbol{u}_j$, p_j within the two fluid layers read

$$\rho_j \partial_t \boldsymbol{u}_j = -\boldsymbol{\nabla}(p_j) + \eta_j \nabla^2 \boldsymbol{u}_j, \tag{2.4}$$

$$\boldsymbol{\nabla} \cdot \boldsymbol{u}_j = 0. \tag{2.5}$$

Eliminating the horizontal velocity and the pressure from (2.4) in the usual way by operating with $\boldsymbol{e}_z \cdot \boldsymbol{\nabla} \times \boldsymbol{\nabla} \times$, we obtain

$$(\partial_t - \nu_j \nabla^2) \nabla^2 w_j = 0, \tag{2.6}$$

where w_j is the vertical velocity in fluid layer j of kinematic viscosity ν_j.

2.2. *Boundary conditions and pressure jump at the interface*

No-slip conditions are imposed at the boundaries $z = -h_1, h_2$, either or both of which may be at infinity. That is, at $z = (-1)^j h_j$,

$$\boldsymbol{u}_j = 0 \Rightarrow w_j = \partial_z w_j = 0. \tag{2.7}$$

The fluid layers are separated by an interface which is initially flat, stationary, and coincident with the $z = 0$ plane by choice of the coordinate system. More generally, after it is destabilized the interface is located at $z = \zeta(\boldsymbol{x}, t)$, where $\boldsymbol{x} \equiv (x, y)$, and obeys the kinematic surface condition (Lamb 1932, §9)

$$[\partial_t + (\boldsymbol{u} \cdot \boldsymbol{\nabla})]\,\zeta = w|_{z=\zeta}, \tag{2.8}$$

which states that the interface is advected by the fluid. All velocity components must be continuous across this interface. Thus at $z = \zeta$ we have

$$\boldsymbol{u}_2 - \boldsymbol{u}_1 = 0 \Rightarrow w_2 - w_1 = \partial_z(w_2 - w_1) = 0. \tag{2.9}$$

Since we are interested in the linear stability of the flat interface, we may Taylor-expand the fields and their z-derivatives around $z = 0$ and retain only the lowest-order terms. It is then sufficient to compute the fields and their vertical derivatives at $z = 0$ instead of at the unknown position of the surface $z = \zeta(\boldsymbol{x}, t)$. This is valid as long as the deformation (ζ) is small compared to the wavelength of the instability and the slope of the deformed interface is much less than unity. The kinematic condition (2.8), linearized and applied at $z = 0$, now reads

$$\partial_t \zeta = w|_{z=0} \tag{2.10}$$

and (2.9) is applied at $z = 0$ as well, greatly simplifying the computations.

The remaining conditions are derived by considering the stress tensor, which is written as

$$\pi_{j,lm} = -(p_j - \rho_j G(t) z)\,\delta_{lm} + \eta_j(\partial_l u_{j,m} + \partial_m u_{j,l}), \tag{2.11}$$

where the indices l, m refer to components x, y, z, and j to the fluid layer.

Any deformation of the flat interface generates viscous stress. For a continuously deformed interface, the tangential components of the stress tensor must also be continuous (Chandrasekhar 1970, §91) at the interface. By setting these equal across the interface, and taking the horizontal divergence of (2.11) dotted with $\boldsymbol{e}_z$, we obtain that at the interface

$$\begin{aligned} &\eta_1(\nabla_H^2 w_1 + \partial_z \boldsymbol{\nabla}_H \cdot \boldsymbol{u}_{H1}) = \eta_2(\nabla_H^2 w_2 + \partial_z \boldsymbol{\nabla}_H \cdot \boldsymbol{u}_{H2}) \\ &\Rightarrow \eta_1(\nabla_H^2 - \partial_{zz}) w_1 = \eta_2(\nabla_H^2 - \partial_{zz}) w_2. \end{aligned} \tag{2.12}$$

The destabilization, and more specifically the curvature, of the interface generates a discontinuity in the normal component of the stress tensor. The jump in the normal component of the stress tensor, for small curvature, is given by

$$\Delta\pi_{zz} = -\sigma\nabla_H^2 \zeta. \tag{2.13}$$

Here $\Delta\chi \equiv \chi|_{z=\zeta+} - \chi|_{z=\zeta-}$ denotes the jump in any quantity χ across the interface, and applies to all quantities to its right within a term. The surface tension coefficient is σ. Substituting the definition (2.11) of the stress tensor into (2.13), we obtain

$$\Delta p = 2\partial_z w|_{z=0}\,\Delta\eta + G(t)\,\zeta\Delta\rho + \sigma\nabla_H^2 \zeta. \tag{2.14}$$

We can derive another expression for the pressure by taking the horizontal divergence of the Navier–Stokes equations (2.4) for each layer:

$$\begin{aligned}\nabla_H^2 p_j &= (\eta_j \nabla^2 - \rho_j \partial_t)\, \boldsymbol{\nabla}_H \cdot \boldsymbol{u}_{Hj} \\ &= (\rho_j \partial_t - \eta_j \nabla^2)\, \partial_z w_j. \end{aligned} \tag{2.15}$$

Setting the discontinuity across the interface of (2.15) equal to the horizontal Laplacian applied to (2.14), we obtain the jump condition (see Appendix A for an alternative derivation) at the interface as

$$\Delta(\rho \partial_t - \eta \nabla^2)\, \partial_z w = 2\nabla_H^2 \partial_z w|_{z=0} \Delta\eta + G(t) \nabla_H^2 \zeta \Delta\rho + \sigma \nabla_H^4 \zeta. \tag{2.16}$$

Equation (2.16) serves as an additional boundary condition for the system (2.6), and is the only equation in which the external forcing $G(t)$ remains explicitly.

Horizontal boundary conditions are required to complete the specification of the stability problem given by (2.6), (2.7), (2.9), (2.10), (2.12) and (2.16). We will consider a horizontally infinite plane, whose normal modes are trigonometric functions, e.g. $\sin(\boldsymbol{k}\cdot\boldsymbol{x})$. The horizontal wavenumber k, where $k^2 = k_x^2 + k_y^2$, can take any real value. We can expand the fields in terms of horizontal normal modes of the Laplacian since the form of the equations is such that each mode is decoupled from the others. This is the approach followed by Benjamin & Ursell (1954) for the ideal fluid case, and it remains valid for the viscous fluid equations in the present case. We now simply replace $w(\boldsymbol{x}, z, t)$ by $\sin(\boldsymbol{k}\cdot\boldsymbol{x})\, w(z, t)$, $\zeta(\boldsymbol{x}, t)$ by $\sin(\boldsymbol{k}\cdot\boldsymbol{x})\, \zeta(t)$, and the differential operator ∇_H^2 by the algebraic one $-k^2$.

The complete linear stability problem is now summarized:

$$[\partial_t - \nu_1(\partial_{zz} - k^2)](\partial_{zz} - k^2) w_1 = 0 \quad \text{for} \quad -h_1 \leqslant z < 0, \tag{2.17}$$

$$[\partial_t - \nu_2(\partial_{zz} - k^2)](\partial_{zz} - k^2) w_2 = 0 \quad \text{for} \quad 0 < z \leqslant h_2. \tag{2.18}$$

The boundary conditions at the two plates are given by

$$w_1 = 0 \quad \text{at} \quad z = -h_1, \tag{2.19}$$

$$w_2 = 0 \quad \text{at} \quad z = h_2, \tag{2.20}$$

$$\partial_z w_1 = 0 \quad \text{at} \quad z = -h_1, \tag{2.21}$$

$$\partial_z w_2 = 0 \quad \text{at} \quad z = h_2, \tag{2.22}$$

and the conditions at the interface are

$$\Delta w = 0, \tag{2.23}$$

$$\Delta \partial_z w = 0, \tag{2.24}$$

$$\Delta\eta(\partial_{zz} + k^2) w = 0, \tag{2.25}$$

$$\Delta[\rho \partial_t - \eta(\partial_{zz} - k^2) + 2\eta k^2]\, \partial_z w = -[\Delta\rho\, G(t) - \sigma k^2] k^2 \zeta. \tag{2.26}$$

The kinematic condition at the interface reads

$$\partial_t \zeta - w|_{z=0} = 0. \tag{2.27}$$

The above set of equations (2.17)–(2.27) constitute the full hydrodynamic system, which we shall refer to as FHS.

3. Floquet solution for the viscous equations

We apply Floquet theory to solve the stability problem (2.17)–(2.27). Because $G(t)$, the gravitational acceleration in the moving frame, is a periodic function of time with period $2\pi/\omega$, the solutions are of Floquet form, i.e.

$$w_j(z, t) = \mathrm{e}^{(\mu + \mathrm{i}\alpha)t}\, \tilde{w}_j(z, t \bmod 2\pi/\omega), \tag{3.1}$$

where $\mu+\mathrm{i}\alpha$ is the Floquet exponent and $\mathrm{e}^{(\mu+\mathrm{i}\alpha)2\pi/\omega}$ is the Floquet multiplier. The function $\tilde{w}_j$ is periodic in time with period $2\pi/\omega$, and may therefore be expanded in the Fourier series

$$\tilde{w}_j(z, t \bmod 2\pi/\omega) = \sum_{n=-\infty}^{\infty} w_{jn}(z)\,\mathrm{e}^{\mathrm{i}n\omega t}. \tag{3.2}$$

The Floquet multipliers are eigenvalues of a real mapping: this implies that they are either real or complex-conjugate pairs. In addition α is defined only modulo ω, since integer multiples of ω may be absorbed into $\tilde{w}_j$. Hence, we restrict consideration to the range $0 \leqslant \alpha \leqslant \frac{1}{2}\omega$. The two cases $\alpha = 0$ and $\alpha = \frac{1}{2}\omega$ are called harmonic and subharmonic, respectively, and correspond to positive or negative real Floquet multipliers, whereas $0 < \alpha < \frac{1}{2}\omega$ corresponds to a complex Floquet multiplier.

The relationship between Fourier modes with positive and negative n depends on the value of α. In the harmonic and subharmonic cases, $\tilde{w}_j$ must obey reality conditions $w_{j,-n} = w^*_{j,n}$ (harmonic) or $w_{j,-n} = w^*_{j,n-1}$ (subharmonic), so that the series (3.2) may be rewritten in terms only of non-negative Fourier indices. If, on the other hand, $0 < \alpha < \frac{1}{2}\omega$, then (3.1) must be added to its complex conjugate in order to form a real field: Fourier coefficients with positive and negative n are independent. Only the harmonic and subharmonic cases are relevant to this linear stability analysis: complex Floquet multipliers are always of magnitude less than or equal to one, and hence do not correspond to growing solutions. This can be shown rigorously for the damped Mathieu equation (H. W. Müller, private communication) and numerically for the Faraday problem for viscous fluids (see below).

The interface position ζ is expanded in the same way:

$$\zeta(t) = \mathrm{e}^{(\mu+\mathrm{i}\alpha)t}\,\tilde{\zeta}(t \bmod 2\pi/\omega), \tag{3.3}$$

$$\tilde{\zeta}(t \bmod 2\pi/\omega) = \sum_{-\infty}^{\infty} \zeta_n\,\mathrm{e}^{\mathrm{i}n\omega t}, \tag{3.4}$$

with the same reality conditions as for w. Equations (2.23) and (2.27) imply that

$$w_{1n}(z=0) = w_{2n}(z=0) = [\mu+\mathrm{i}(\alpha+n\omega)]\,\zeta_n. \tag{3.5}$$

Substituting (3.1) and (3.2) into (2.17) and (2.18), we obtain for each layer j and for each Fourier component n the fourth-order ordinary differential equation in z:

$$[\mu+\mathrm{i}(\alpha+n\omega)-\nu_j(\partial_{zz}-k^2)](\partial_{zz}-k^2)\,w_{jn} = 0, \tag{3.6}$$

with solutions

$$w_{jn}(z) = a_{jn}\,\mathrm{e}^{kz} + b_{jn}\,\mathrm{e}^{-kz} + c_{jn}\,\mathrm{e}^{q_{jn}z} + d_{jn}\,\mathrm{e}^{-q_{jn}z}, \tag{3.7}$$

where

$$q^2_{jn} \equiv k^2 + \frac{\mu+\mathrm{i}(\alpha+n\omega)}{\nu_j}, \tag{3.8}$$

with the convention that q_{jn} is the root of (3.8) with positive real part.

For each n, the seven boundary and continuity conditions (2.19)–(2.25) relate the eight coefficients in (3.7). Most conveniently, the conditions can be used to express all of the coefficients as multiples of ζ_n via (3.5). (The algebra is straightforward but tedious and, especially for layers of finite height, is carried out numerically or symbolically; see Appendix B.) The case $\mu+\mathrm{i}(\alpha+n\omega) = 0$ is slightly different: the functions $z\,\mathrm{e}^{\pm kz}$ replace $\mathrm{e}^{\pm q_{jn}z}$ in the solution (3.7). If ζ is of Floquet form (3.3), then (3.5) implies that $w_{j0}(z=0) = 0$ when $\mu+\mathrm{i}(\alpha+n\omega) = 0$, which, together with the boundary and continuity conditions, ensures that $w_{j0}(z) = 0$ for all z.

The only one of the equations which couples the different Fourier modes is the pressure jump condition (2.26) which we now express for each mode as

$$\Delta[\rho\{\mu+\mathrm{i}(\alpha+n\omega)\}+3\eta k^2]\,\partial_z w_n-\Delta\eta\,\partial_{zzz} w_n+(\Delta\rho g-\sigma k^2)\,k^2\,\zeta_n=\Delta\rho k^2\,[f(t)\,\tilde{\zeta}(t)]_n. \quad (3.9)$$

In (3.9), the notation $[f(t)\,\tilde{\zeta}(t)]_n$ denotes the nth Fourier component of the product. For single-frequency forcing, we have

$$f(t)=\tfrac{1}{2}a(\mathrm{e}^{\mathrm{i}\omega t}+\mathrm{e}^{-\mathrm{i}\omega t}), \quad (3.10)$$

leading to

$$[f(t)\,\tilde{\zeta}(t)]_n=\tfrac{1}{2}a(\zeta_{n+1}+\zeta_{n-1}). \quad (3.11)$$

Recalling that $\partial_z w_n(0)$ and $\partial_{zzz} w_n(0)$ can be expressed as multiples of ζ_n, the entire left-hand side of (3.9) can be written as $\tfrac{1}{2}\Delta\rho k^2 A_n\,\zeta_n$, with $A_n=A_n^r+\mathrm{i}A_n^i$ complex. The jump condition can then be rewritten as

$$A_n\,\zeta_n=a(\zeta_{n+1}+\zeta_{n-1}). \quad (3.12)$$

The reality conditions

$$\zeta_{-1}=\zeta_1^* \quad \text{(harmonic)} \quad (3.13)$$

or

$$\zeta_{-1}=\zeta_0^* \quad \text{(subharmonic)} \quad (3.14)$$

and truncation of the Fourier series (3.4) are used to restrict consideration to $0\leqslant n\leqslant N$.

The coefficients A_n and hence the system (3.12) depend on the Floquet exponent $\mu+\mathrm{i}\alpha$ via (3.8) and the boundary conditions (see Appendix B) in a complicated manner. However, the amplitude a of the external forcing appears linearly. In fact, for fixed Floquet exponent, (3.12) can be considered to be an eigenvalue problem with eigenvalues a and eigenvectors whose components are the real and imaginary parts of the ζ_n. That is, we write (3.12) as the generalized eigenvalue problem

$$\boldsymbol{A}\boldsymbol{\zeta}=a\boldsymbol{B}\boldsymbol{\zeta}. \quad (3.15)$$

In (3.15), $\boldsymbol{A}$ is a diagonal complex matrix and $\boldsymbol{B}$ is a banded matrix whose structure depends on α. In the harmonic case, we have

$$\begin{pmatrix} A_0^r & -A_0^i & 0 & 0 & 0 & 0 & \cdots \\ A_0^i & A_0^r & 0 & 0 & 0 & 0 & \cdots \\ 0 & 0 & A_1^r & -A_1^i & 0 & 0 & \cdots \\ 0 & 0 & A_1^i & A_1^r & 0 & 0 & \cdots \\ 0 & 0 & 0 & 0 & A_2^r & -A_2^i & \cdots \\ 0 & 0 & 0 & 0 & A_2^i & A_2^r & \cdots \\ \vdots & \vdots & \vdots & \vdots & \vdots & \vdots & \vdots \end{pmatrix} \begin{pmatrix} \zeta_0^r \\ \zeta_0^i \\ \zeta_1^r \\ \zeta_1^i \\ \zeta_2^r \\ \zeta_2^i \\ \vdots \end{pmatrix} = a \begin{pmatrix} 0 & 0 & 2 & 0 & 0 & 0 & \cdots \\ 0 & 0 & 0 & 0 & 0 & 0 & \cdots \\ 1 & 0 & 0 & 0 & 1 & 0 & \cdots \\ 0 & 1 & 0 & 0 & 0 & 1 & \cdots \\ 0 & 0 & 1 & 0 & 0 & 0 & \cdots \\ 0 & 0 & 0 & 1 & 0 & 0 & \cdots \\ \vdots & \vdots & \vdots & \vdots & \vdots & \vdots & \vdots \end{pmatrix} \begin{pmatrix} \zeta_0^r \\ \zeta_0^i \\ \zeta_1^r \\ \zeta_1^i \\ \zeta_2^r \\ \zeta_2^i \\ \vdots \end{pmatrix}, \quad (3.16)$$

and in the subharmonic case, we have

$$\begin{pmatrix} A_0^r & -A_0^i & 0 & 0 & 0 & 0 & \cdots \\ A_0^i & A_0^r & 0 & 0 & 0 & 0 & \cdots \\ 0 & 0 & A_1^r & -A_1^i & 0 & 0 & \cdots \\ 0 & 0 & A_1^i & A_1^r & 0 & 0 & \cdots \\ 0 & 0 & 0 & 0 & A_2^r & -A_2^i & \cdots \\ 0 & 0 & 0 & 0 & A_2^i & A_2^r & \cdots \\ \vdots & \vdots & \vdots & \vdots & \vdots & \vdots & \vdots \end{pmatrix} \begin{pmatrix} \zeta_0^r \\ \zeta_0^i \\ \zeta_1^r \\ \zeta_1^i \\ \zeta_2^r \\ \zeta_2^i \\ \vdots \end{pmatrix} = a \begin{pmatrix} 1 & 0 & 1 & 0 & 0 & 0 & \cdots \\ 0 & -1 & 0 & 1 & 0 & 0 & \cdots \\ 1 & 0 & 0 & 0 & 1 & 0 & \cdots \\ 0 & 1 & 0 & 0 & 0 & 1 & \cdots \\ 0 & 0 & 1 & 0 & 0 & 0 & \cdots \\ 0 & 0 & 0 & 1 & 0 & 0 & \cdots \\ \vdots & \vdots & \vdots & \vdots & \vdots & \vdots & \vdots \end{pmatrix} \begin{pmatrix} \zeta_0^r \\ \zeta_0^i \\ \zeta_1^r \\ \zeta_1^i \\ \zeta_2^r \\ \zeta_2^i \\ \vdots \end{pmatrix}. \quad (3.17)$$

The usual procedure for a stability analysis is to fix the wavenumber k and the amplitude a (as well as the other hydrodynamic parameters), to calculate the exponents $\mu+\mathrm{i}\alpha$, and to select that whose growth rate $\mu(k,a)$ is largest. The curves in the (k,a) plane on which $\mu(k,a)=0$ are the marginal stability boundaries, determined by interpolating a between positive and negative values of μ. In the present method, we instead fix $\mu+\mathrm{i}\alpha$, usually at $\mu=0$ and at $\alpha=\frac{1}{2}\omega$ or $\alpha=0$. We then solve (3.15) for the eigenvalues a. Only real and positive values of a are meaningful in this context. (For single-frequency forcing, the eigenvalues occur in $+/-$ pairs because the symmetry $f(t)=f(t+\pi/\omega)$ implies that, if $(a,\zeta(t))$ is a solution, then so is $(-a,\zeta(t+\pi/\omega))$). We select the smallest, or several smallest, real positive eigenvalues a. These give the marginal stability boundaries $a(k,\mu=0,\ \alpha=\frac{1}{2}\omega)$ and $a(k,\mu=0,\ \alpha=0)$ directly without interpolation (see figure 1). If we set $\mu=0$ and $0<\alpha<\frac{1}{2}\omega$, we find only complex a, indicating that the modes with complex Floquet multipliers are damped as stated previously. The critical amplitude a_c is the smallest value of a on the marginal stability boundaries, and the corresponding wavenumber is the critical wavenumber k_c. It is this wavenumber which will be excited by gradually raising the forcing amplitude a, if, as we have assumed, the system is horizontally infinite and has access to all wavenumbers.

An ordinary eigenvalue problem can easily be constructed from (3.15) by inverting $\boldsymbol{A}$:

$$\boldsymbol{A}^{-1}\boldsymbol{B}\zeta=\frac{1}{a}\zeta. \tag{3.18}$$

In cases for which $\boldsymbol{A}$ is singular (as occurs in inviscid fluids at onset: see §4) but $\boldsymbol{B}$ is not (as in the subharmonic case), the latter can be inverted instead:

$$\boldsymbol{B}^{-1}\boldsymbol{A}\zeta=a\zeta. \tag{3.19}$$

Eigenproblems (3.18) or (3.19) are solved straightforwardly by constructing the corresponding matrix, diagonalizing it via EISPACK, and selecting the smallest, or several smallest, real positive values of a. More specifically we calculate the values A_n corresponding to our hydrodynamic parameters, and then multiply all possible unit vectors ζ successively by $\boldsymbol{B}$ and by $\boldsymbol{A}^{-1}$ (for (3.18)) or by $\boldsymbol{A}$ and by $\boldsymbol{B}^{-1}$ (for (3.19)). Note that $\boldsymbol{B}$ is not a complex matrix: compare the first two rows of $\boldsymbol{B}$ in (3.16) or (3.17) with the 2×2 blocks of $\boldsymbol{A}$ and of the rest of $\boldsymbol{B}$. This is a consequence of the reality conditions (3.13) or (3.14), which state that $\boldsymbol{B}$ acts on ζ^* as well as ζ. Thus, $\boldsymbol{A}^{-1}\boldsymbol{B}$ and $\boldsymbol{B}^{-1}\boldsymbol{A}$ are $2(N+1)\times 2(N+1)$ real matrices, and subroutine rg (Real General) is called to diagonalize them.

Formulation (3.18) has a slight advantage over (3.19). Inversion of $\boldsymbol{A}$ requires only one complex division per Fourier mode, whereas inversion of the banded matrix $\boldsymbol{B}$ requires an LU decomposition. For one-frequency forcing we find that a temporal resolution of $N=5$ or $N=10$ is sufficient, and diagonalization of the resulting 12×12 or 22×22 matrices on a SUN Sparc-4 is rapidly performed. Research currently being undertaken by the present authors with W. S. Edwards shows that the above method is quite general and equally applicable to a general periodic forcing function.

4. Ideal fluids

4.1. *Derivation of the Mathieu equation*

For two ideal fluids ($\nu_j = 0$), the hydrodynamic equations reduce to

$$\partial_t(\partial_{zz}-k^2)\,w_1 = 0 \quad \text{for} \quad -h_1 \leqslant z < 0, \tag{4.1}$$

$$\partial_t(\partial_{zz}-k^2)\,w_2 = 0 \quad \text{for} \quad 0 < z \leqslant h_2. \tag{4.2}$$

The boundary conditions at the plates become

$$w_1 = 0 \quad \text{at} \quad z = -h_1, \tag{4.3}$$

$$w_2 = 0 \quad \text{at} \quad z = h_2, \tag{4.4}$$

and those at the interface read

$$\Delta w = 0, \tag{4.5}$$

$$\Delta\rho\,\partial_t\partial_z w = [\Delta\rho(g - a\cos(\omega t)) - \sigma k^2]k^2\zeta, \tag{4.6}$$

$$\partial_t\zeta - w|_{z=0} = 0. \tag{4.7}$$

The horizontal velocity may be discontinuous across the interface, leading to discontinuity in $\partial_z w$. Equations (4.1) and (4.2) state that the vorticity remains constant over time. One usually makes the additional assumption for ideal fluids that the initial vorticity is zero, leading to

$$(\partial_{zz}-k^2)\,w_j = 0. \tag{4.8}$$

Solutions to (4.8) that satisfy boundary conditions (4.3)–(4.5) for the simplest case of two fluid layers of infinite heights are

$$w_1(z,t) = W(t)\,\mathrm{e}^{kz} \quad \text{for} \quad -\infty \leqslant z < 0, \tag{4.9}$$

$$w_2(z,t) = W(t)\,\mathrm{e}^{-kz} \quad \text{for} \quad 0 < z \leqslant \infty. \tag{4.10}$$

The quantities appearing in the pressure jump condition (4.6) can then be calculated and are given by

$$\dot{\zeta}(t) = W(t), \tag{4.11}$$

$$\Delta\rho\,\partial_t\partial_z w = -k(\rho_1+\rho_2)\,\dot{W}(t). \tag{4.12}$$

Substituting these into (4.6) we arrive at

$$\ddot{\zeta} + \omega_0^2[1 - \hat{a}\cos(\omega t)]\,\zeta = 0, \tag{4.13}$$

where

$$\omega_0^2 = \frac{(\rho_1-\rho_2)\,gk + \sigma k^3}{\rho_1+\rho_2} \tag{4.14}$$

and

$$\hat{a} = \frac{(\rho_1-\rho_2)\,ak}{(\rho_1+\rho_2)\,\omega_0^2}. \tag{4.15}$$

For fluid layers of finite heights, $\rho_1+\rho_2$ in the denominator in (4.14) and (4.15) is simply replaced by $[\rho_1 \coth(kh_1) + \rho_2 \coth(kh_2)]$. When $h_1 = h_2$ and $\rho_2 = 0$, this reproduces the original ideal fluid result of Benjamin & Ursell (1954).

4.2. *Incorporation of damping*

For small damping (i.e. for $\lambda^2\omega \gg \nu$) and for small deformation of the interface ($\zeta \ll \lambda$), the flow can be considered to be irrotational except for a thin layer around the interface. Neglecting this thin layer and the viscous boundary conditions, we can

estimate the viscous damping using the ideal fluid velocities, which, for two fluids of infinite height, are given by

$$\boldsymbol{u}(\boldsymbol{x}, z, t) = [\boldsymbol{e}_z \sin(\boldsymbol{k}\cdot\boldsymbol{x}) \mp \frac{\boldsymbol{k}}{k} \cos(\boldsymbol{k}\cdot\boldsymbol{x})]\, W(t)\, \mathrm{e}^{\mp kz}, \tag{4.16}$$

where the $\mp$ signs are used for the upper and lower layers and $\boldsymbol{k}$ is the horizontal wavevector. The damping coefficient γ is defined (Landau & Lifshitz 1987, §25) as

$$\gamma = |\bar{\dot{E}}|/2\bar{E}, \tag{4.17}$$

where $\bar{\dot{E}}$ and $\bar{E}$ are time-averaged values of the rate of dissipation of the total mechanical energy due to viscosity and the total mechanical energy, to be estimated as follows.

Following the argument of Landau & Lifshitz (1987, §25) the time-averaged mechanical energy, for the case of two fluids, is given by the sum of volume integrals

$$\bar{E} = \rho_1 \int \overline{(u_{1,m})^2}\, \mathrm{d}v_1 + \rho_2 \int \overline{(u_{2,m})^2}\, \mathrm{d}v_2 \tag{4.18}$$

and the time-averaged rate of dissipation is

$$\bar{\dot{E}} = -2\left(\eta_1 \int \overline{(\partial_l u_{1,m})^2}\, \mathrm{d}v_1 + \eta_2 \int \overline{(\partial_l u_{2,m})^2}\, \mathrm{d}v_2\right). \tag{4.19}$$

In (4.18) and (4.19), the first integral is to be evaluated in the lower fluid, and the second in the upper fluid. The indices l, m refer to components x, y, z and sums over these indices are implied. Combining (4.16)–(4.19), we find

$$\gamma = 2k^2 \frac{\eta_1 + \eta_2}{\rho_1 + \rho_2}. \tag{4.20}$$

For fluids of finite depths, the terms $\eta_1 + \eta_2$ and $\rho_1 + \rho_2$ in (4.20) are replaced by $[\eta_1 \coth(kh_1) + \eta_2 \coth(kh_2)]$ and $[\rho_1 \coth(kh_1) + \rho_2 \coth(kh_2)]$ respectively.

Traditionally, for low-viscosity fluids, a linear damping term (e.g. Ciliberto & Gollub 1985) is added to the Mathieu equation to account for viscous dissipation. We do the same here for the two-fluid case in order to compare the results of the full hydrodynamic system (FHS) with this phenomenological approach. However, our damping is wavenumber dependent. The resulting equation is

$$\ddot{\zeta} + 2\gamma\dot{\zeta} + \omega_0^2(1 - \hat{a}\cos\omega t)\,\zeta = 0. \tag{4.21}$$

We shall refer to (4.21) with parameter values given by (4.14) and (4.20) or its finite-depth version as the model.

It is sometimes convenient to remove the damping from (4.21) by the transformation

$$\zeta \equiv \mathrm{e}^{-\gamma t}\, \zeta_d. \tag{4.22}$$

Insertion of (4.22) into (4.21) results in the standard Mathieu equation

$$\ddot{\zeta}_d + \omega_d^2(1 - \hat{a}_d \cos\omega t)\,\zeta_d = 0, \tag{4.23}$$

where

$$\omega_d^2 \equiv \omega_0^2 - \gamma^2, \tag{4.24}$$

$$\hat{a}_d \equiv \hat{a}\omega_0^2/\omega_d^2. \tag{4.25}$$

We solve the damped Mathieu equation (4.21) numerically by a simplified version of the technique used to solve the full hydrodynamic problem. We substitute the Floquet form (3.3) and (3.4) into (4.21) and obtain

$$[\{\mu + \mathrm{i}(\alpha + n\omega)\}^2 + 2\gamma\{\mu + \mathrm{i}(\alpha + n\omega)\} + \omega_0^2]\,\zeta_n = \tfrac{1}{2}\omega_0^2\,\hat{a}(\zeta_{n-1} + \zeta_{n+1}), \tag{4.26}$$

which is of the same form as (3.12). The matrices $\boldsymbol{B}$ are exactly as in (3.16) and (3.17), whereas the matrix $\boldsymbol{A}$ has coefficients given explicitly by

$$A_n = \frac{2}{\omega_0^2}[\{\mu + \mathrm{i}(\alpha + n\omega)\}^2 + 2\gamma\{\mu + \mathrm{i}(\alpha + n\omega)\} + \omega_0^2]. \tag{4.27}$$

From the form of (4.26) and (4.27), we easily obtain the condition for resonance for infinitesimal forcing amplitude. Setting $\hat{a} = 0$, $\mu = 0$, we see that the existence of a non-trivial solution to (4.26) requires that $A_n = 0$ for some n, i.e.

$$-(\alpha + n\omega)^2 + \omega_0^2 = 0, \tag{4.28}$$

$$2\gamma(\alpha + n\omega) = 0. \tag{4.29}$$

We conclude that, in fact, $\gamma = 0$ if there is an instability for $\hat{a} = 0$ and

$$\alpha + n\omega = \omega_0. \tag{4.30}$$

Finally, using $\alpha = 0$ or $\alpha = \frac{1}{2}\omega$, we arrive at the usual result:

$$\omega_0 = \tfrac{1}{2}m\omega, \tag{4.31}$$

where m is odd for subharmonic resonance and even for harmonic resonance.

5. Results

We determined the stability of the flat interface to standing waves of wavenumber k as a function of the amplitude a of the external acceleration. In figure 1, we show the neutral stability curves that divide the (a, k)-plane into a region of stable solutions, and regions, called tongues, of unstable (growing) harmonic or subharmonic solutions. The harmonic solutions have the same period as that of the external driving and the subharmonic solutions have a period twice that of the external driving. We show the stability boundaries obtained by Floquet analysis of the Mathieu equation (4.13)–(4.15) derived from the ideal fluid equations in figure 1(*a*). Tongues of harmonic and subharmonic response alternate. As a approaches zero, the temporal dependence of the response ζ corresponding to the mth tongue approaches a single Fourier mode $\mathrm{e}^{\mathrm{i}m\omega t/2}$. For higher a, ζ is a superposition of different frequencies. However, harmonic and subharmonic responses remain separated: ζ contains frequencies which are either all odd or all even multiples of $\frac{1}{2}\omega$, as can be seen from the Floquet form (3.3) and (3.4). In the ideal fluid case, where $a_c = 0$ for all tongues, modes from different tongues can be excited even for infinitesimally small a. In figure 1 (*a*), where the excitation frequency ($= \omega/2\pi$) is 100 Hz, the response frequencies at onset for the first three tongues are 50, 100 and 150 Hz, respectively.

In figure 1 (*b*), we present the stability boundaries obtained by Floquet analysis of the FHS for viscous fluids (here, $\nu_1 = \nu_2 = 7.516 \times 10^{-8}$ m^2 s^{-1}). The viscosity smooths the bottom of the tongues, widening the band of excited wavenumbers k. The minima (k_c, a_c) are displaced towards higher k and a. Since the viscous dissipation increases with k, a_c is also higher for larger k. Because the lowest tongue is subharmonic, the interface is excited subharmonically at onset. Since a_c is always finite in the presence of viscosity, the solutions at onset are superpositions of many frequencies. In the inset of figure 1 (*b*), the lower parts of the neutral stability curves for the model ((4.21) with (4.14), (4.15) and (4.20)) and the FHS are compared. The model (dashed curve) has a higher threshold a_c and a lower critical wavenumber k_c than does the FHS (solid curve) for the present case.

To study the influence of viscosity in more detail, we plot the critical wavelength $\lambda_c (= 2\pi/k_c)$ and the critical excitation amplitude a_c as a function of kinematic viscosity

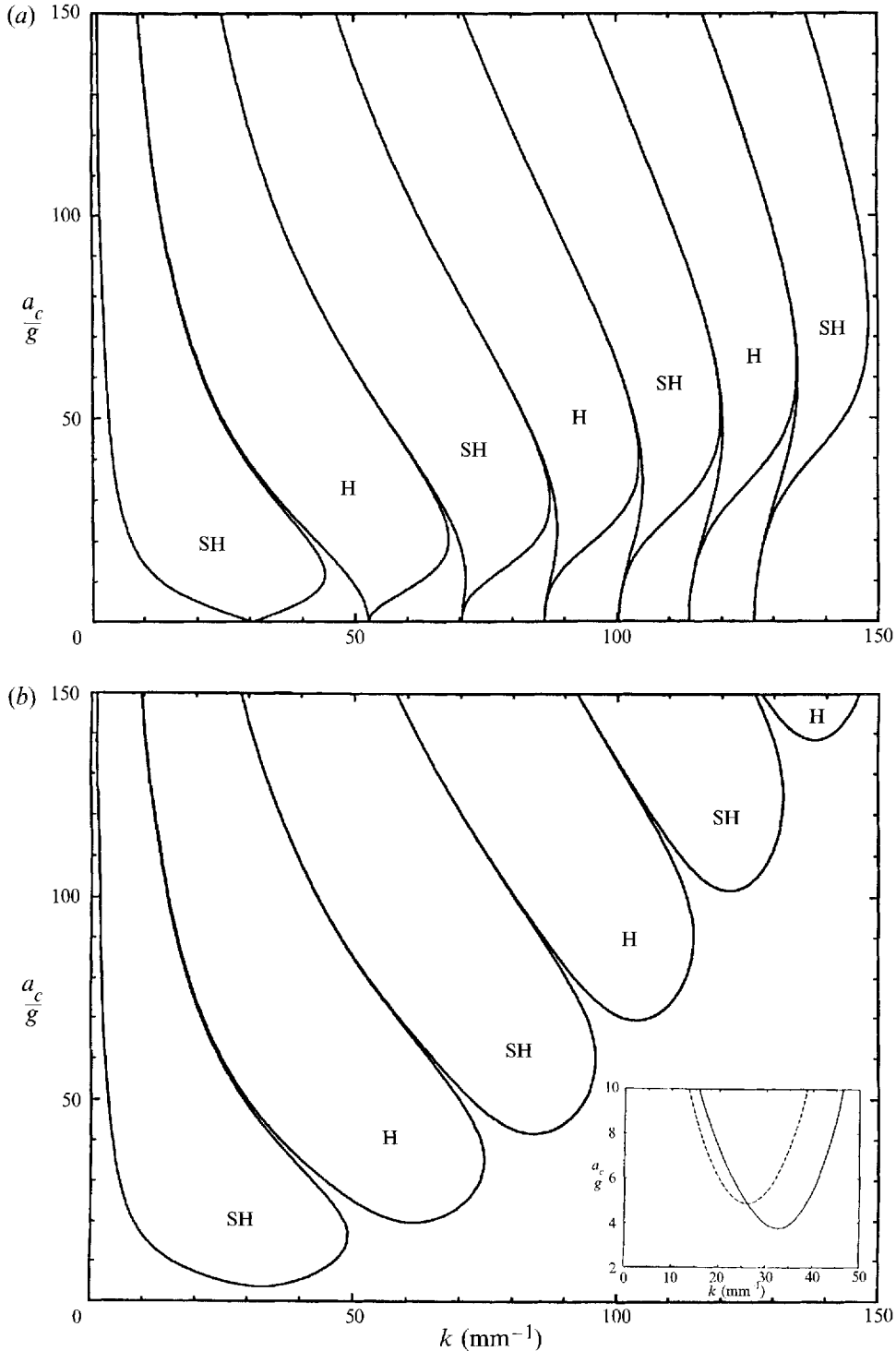

FIGURE 1. (*a*) Stability boundary for ideal fluids. The tongues correspond alternately to subharmonic (SH) and harmonic (H) responses. Fluid parameters are $\rho_1 = 519.933$ Kg m^{-3}, $\rho_2 = 415.667$ Kg m^{-3}, $\sigma = 2.181 \times 10^{-6}$ n m^{-2} and $2\pi/\omega = 100$ Hz. (*b*) Stability boundary for FHS. $\eta_1 = 3.908 \times 10^{-5}$ Pa s, $\eta_2 = 3.124 \times 10^{-5}$ Pa s, and other parameters are as in (*a*). Inset: Comparison of the lowest tongues for the model (dashed line) and the FHS (solid line).

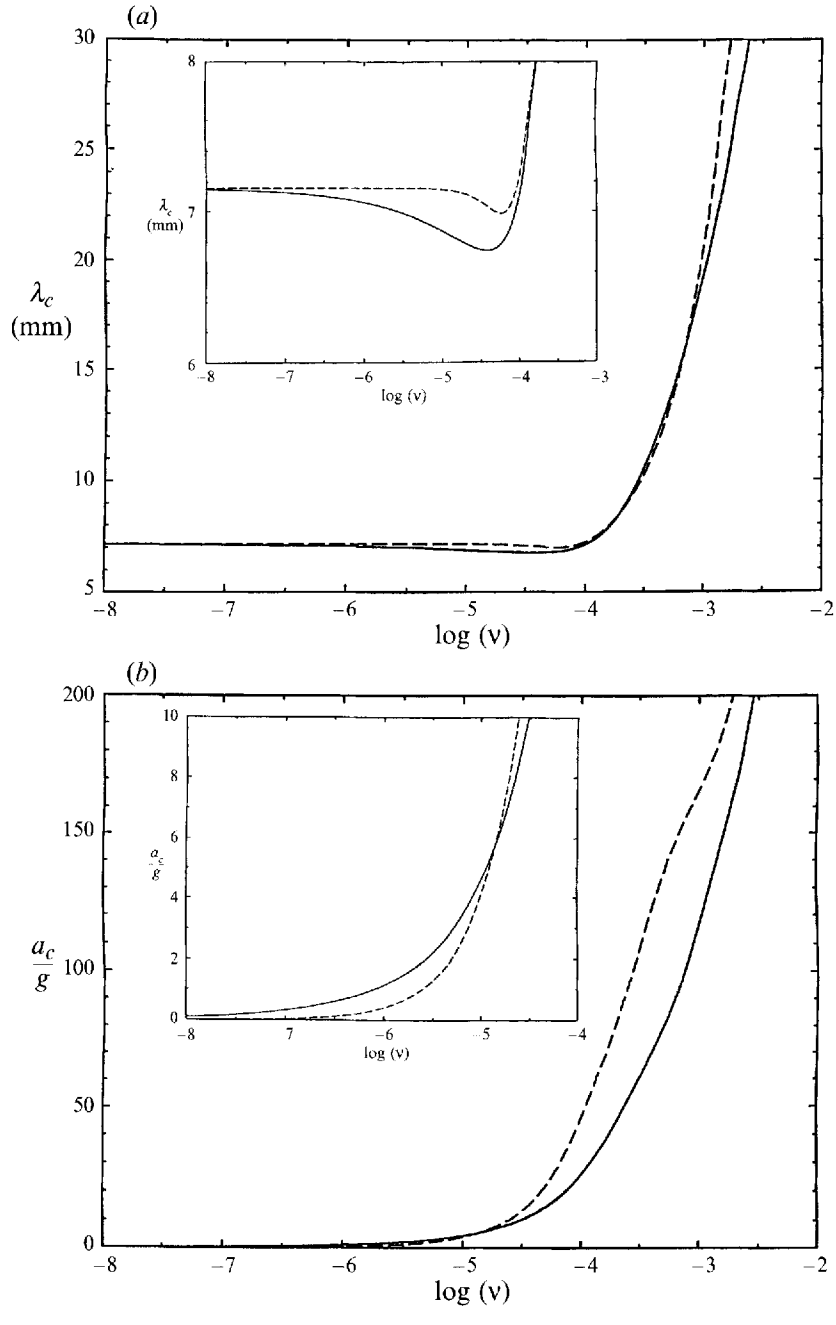

FIGURE 2. (*a*) Wavelength λ_c at onset as a function of viscosity ν. The prediction of the model (dashed line) is generally above that of the FHS (solid line). Parameters are $\rho_1 = 10^3$ Kg m^{-3}, $\rho_2 = 0.5 \times \rho_1$, $\sigma = 72.5 \times 10^{-3}$ nm^{-1} and $\omega/2\pi = 60$ Hz. $\nu = \nu_1 = \nu_2$ is in units of m^2 s^{-1}. (*b*) Stability threshold a_c as a function of viscosity ν. The model (dashed line) greatly underestimates the stability threshold for small viscosity and overestimates it for higher viscosity.

ν for both the FHS and the model in figure 2. We have set $\nu_1 = \nu_2$, which does not obscure the essential features of the problem. The assumption of infinite fluid depths serves to focus the comparison of the viscous stresses at the interface, avoiding the effect of additional stresses at the upper and lower plates.

At very low viscosity, figure 2(*a*) shows that the wavelengths predicted by the FHS and by the model both converge to that given by the dispersion relation (4.14) for ideal fluids, as expected. As ν increases from zero, we see that λ_c first decreases (inset, figure 2*a*) slightly and then increases strongly. Since the wavelengths predicted by the model and FHS do not differ significantly for low viscosity, we may use the model as a tool to understand the initial decrease in λ_c with increasing ν. The response function, for small damping, may be considered to be dominated by frequency ω_d, which is half the excitation frequency ω. Therefore, from the dispersion relation given by (4.24), we have:

$$(\tfrac{1}{2}\omega)^2 \approx \omega_d^2(k) = \frac{(\rho_1-\rho_2)\,gk+\sigma k^3}{\rho_1+\rho_2} - \left(2k^2\frac{\eta_1+\eta_2}{\rho_1+\rho_2}\right)^2. \tag{5.1}$$

For fixed ω, (5.1) has one real root k for $\eta_1 = \eta_2 = 0$, $\rho_1 \geqslant \rho_2$. For finite viscosity, there are two real roots, but only the smaller one is relevant, and it can be seen that this root k_c increases with $\eta_1+\eta_2$. Consequently λ_c decreases with increasing viscosity. For higher viscosity, we see from figure 2(*a*) that the selected wavelength λ_c begins to increase strongly with viscosity. Since the viscous dissipation is much stronger at higher viscosity, the system prefers smaller k_c, i.e. larger λ_c, to minimize the viscous dissipation. Another way of seeing this is that the viscous timescale $\tau_{vis}(\approx \lambda_c^2/\nu)$ becomes comparable to the typical timescale of the response $\tau_r(\approx 4\pi/\omega)$ and the wavelength selection is strongly affected.

Figure 2(*b*) shows the stability threshold a_c as a function of viscosity. Since the model neglects the viscous boundary conditions at the interface, it grossly underestimates the energy dissipated – and therefore the threshold – at small viscosities (inset, figure 2*b*). Even a thin boundary layer at the interface costs considerable energy: it is necessary to consider the viscous boundary condition in order to predict the stability threshold. At higher viscosity, viscous dissipation can no longer be treated as a perturbation, and the flow should be considered rotational. Assumptions inherent in the model – for example the use of the ideal fluid solutions in expressions (4.18) and (4.19) for the energy and its dissipation – are no longer valid. From figure 2(*b*), we see that the model overestimates the stability threshold for larger viscosity.

We compare the results of the FHS and of the model to experimental results obtained in a viscous glycerine–water mixture (Edwards & Fauve 1993) in contact with air. The experiment uses the 'rim-full' technique (Benjamin & Scott 1979; Douady 1990) to pin the surface of the liquid to the edge of the vessel. This also makes the surface flat (i.e. free from any meniscus) before instability sets in. We consider the glycerine–water mixture to be a layer of finite height $h = 0.29$ cm, in contact with a layer of air of infinite height. In figure 3, we plot the experimental data for the critical wavelength λ_c and amplitude a_c as a function of forcing frequency. The solid and dashed curves are obtained from the FHS and from the model with finite depth corrections, respectively. We note, however, that the values for the surface tension σ and the viscosity ν were chosen so as to best fit the FHS to the experimental data. This led to values $\sigma = 67.6\times10^{-3}$ n m^{-1} and $\nu = 1.02\times10^{-4}$ m^2 s^{-1}, which are in good agreement with the corresponding values given in the literature for the mixture, composed of 88% (by weight) glycerol and 12% water, at temperature 23 °C. With these values, both the model and the FHS agree reasonably well with the experimentally measured wavelengths. The experimentally measured amplitudes agree quite well with the FHS over the entire frequency range, and not at all with the model. *It is impossible to improve the fit of the critical amplitudes to the model by varying σ and ν.*

We now compare the results of the FHS with the experiments of Fauve *et al.* (1992)

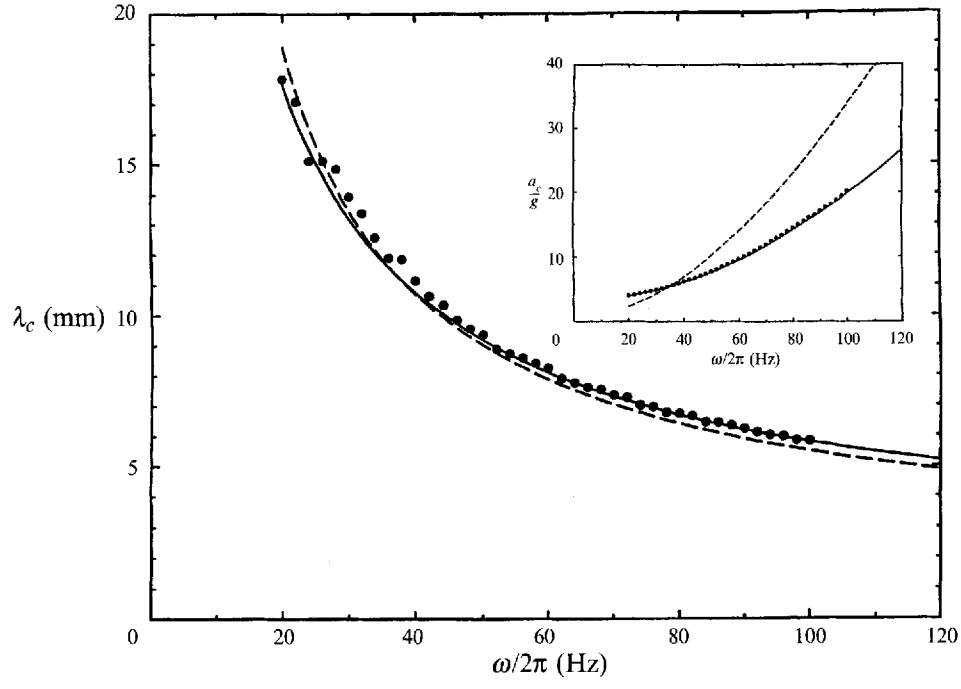

FIGURE 3. Dispersion relation for glycerine–water mixture in contact with air at atmospheric pressure. Fitting the experimental data (Edwards & Fauve 1993) with the results of the FHS (solid lines) leads to $\sigma = 67.6 \times 10^{-3}$ nm^{-1}. Inset: Fitting of the experimental data for the stability threshold leads to $\nu = 1.02 \times 10^{-4}$ m^2 s^{-1}.

for carbon dioxide (CO_2) near the L–V critical point. This proves to be much more difficult, owing to uncertainties in almost all of the fluid parameters. We need the values of the densities ρ_{liq}, ρ_{vap}, and the dynamic viscosities η_{liq}, η_{vap} of the two phases of CO_2 and the coefficient of surface tension σ of the interface as a function of the temperature difference $\Delta T(= T_c - T)$ in order to be able to compare our prediction with the experimental results. The density difference $\rho_{liq} - \rho_{vap}$ between the two phases is known (see for instance Moldover 1985 and references therein) with reasonable accuracy ($< 2\%$) and can be computed using the power law

$$\rho_{liq} - \rho_{vap} = 2\rho_c B_0 t^{\beta}(1 + B_1 t^{\delta}), \tag{5.2}$$

where $t = (T_c - T)/T_c$, $\beta = 0.325$ and $\delta = 0.5$. For CO_2 we used $B_0 = 1.60$, $B_1 = 1.454$, $\rho_c = 467.8$ Kg m^{-3} and $T_c = 304.13$ K. The sum $\rho_{liq} + \rho_{vap}$ of the two phases approaches $2\rho_c$ as T approaches T_c, but its exact dependence on ΔT is not known. The surface tension σ and the sum $(\eta_{liq} + \eta_{vap})$ of dynamic viscosities for CO_2 have been measured experimentally for $0.012 \leqslant \Delta T \leqslant 12$ K by Herpin & Meunier (1974). Herpin & Meunier (1974) also observed that the kinematic viscosities ν_{liq}, ν_{vap} of both phases remain roughly equal near the L–V critical point in many liquid–vapour systems, including CO_2. Utilizing this fact, we can express the dynamic viscosity of one phase in terms of that of the other, and of the two densities. We treat the sum $\rho_{liq} + \rho_{vap}$ of the densities of two phases, the surface tension σ and the dynamic viscosity of one phase (say, η_{liq}) as free parameters. The infinite depth limit is a reasonable approximation for this experiment.

In figure 4, we compare the dispersion relations and the stability threshold a_c of the

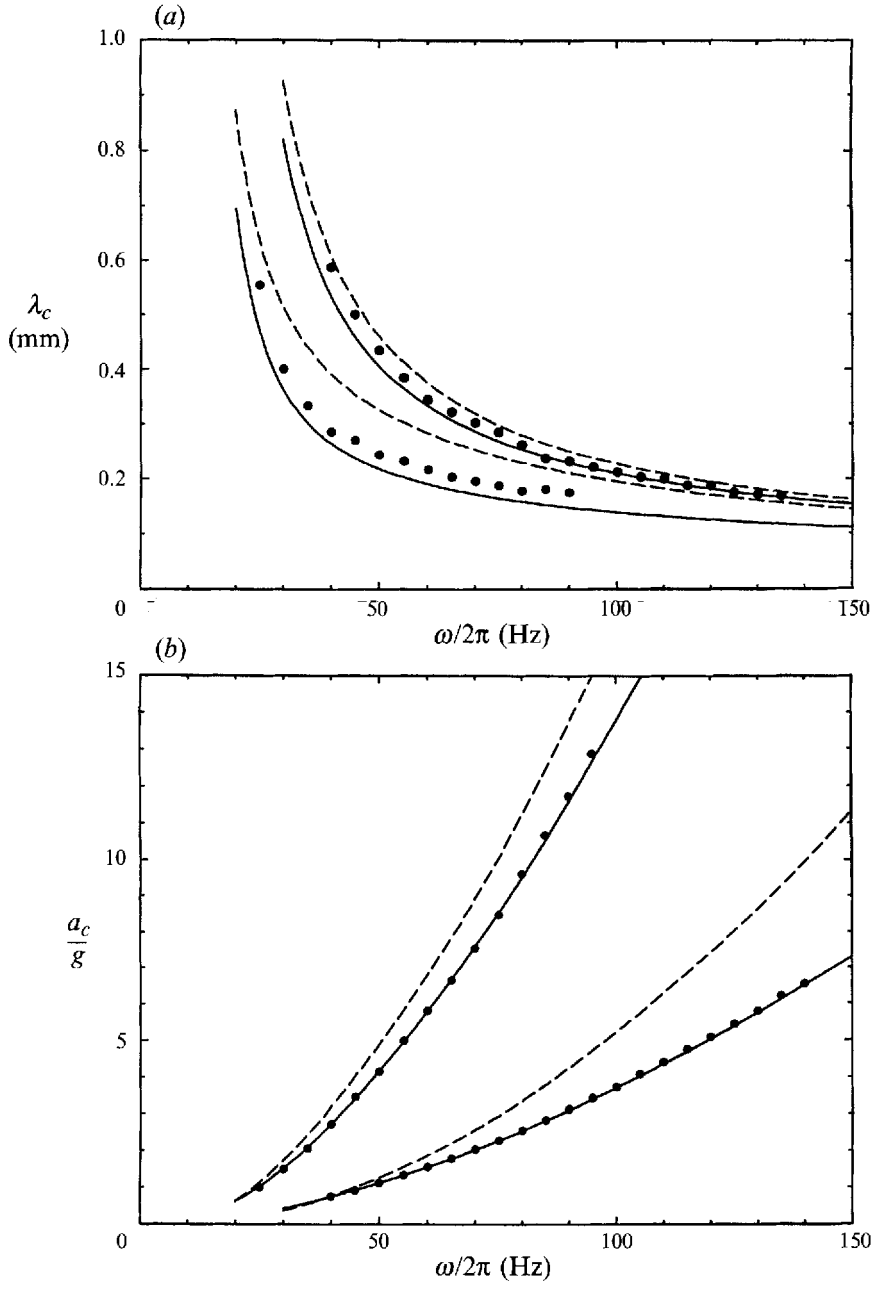

FIGURE 4. (*a*) Comparison of dispersion relations for liquid–vapour interface of CO_2. Experimental results (filled circles) of Fauve *et al.* (1992), results of the FHS (solid lines) and the predictions of the model (dashed lines) are for $\Delta T = 0.078$ K (upper set of curves) and for $\Delta T = 0.007$ K (lower set of curves). (*b*) Comparison of stability threshold for CO_2. Experimental results (filled circles) of Fauve *et al.* (1992), results of the FHS (solid lines) and the results of the model (dashed lines) are for $\Delta T = 0.078$ K (lower set of curves) and for $\Delta T = 0.007$ K (upper set of curves).

FHS (solid line) and of the model (dashed line) with that of the experiment. Choosing the free parameters to best fit the results of the FHS to the experimental data led, for $\Delta T = 0.078$ K, to the values $\rho_{liq} = 501.22$ Kg m^{-3}, $\rho_{vap} = 396.95$ Kg m^{-3}, $\sigma = 2.79 \times 10^{-6}$ n m^{-1}, $\eta_{liq} = 4.17 \times 10^{-5}$ Pa s and $\eta_{vap} = 3.30 \times 10^{-5}$ Pa s. The resulting

value for the sum $\eta_{liq}+\eta_{vap}$ is in excellent agreement with the values measured by Herpin & Meunier (1974), while σ is in fairly good agreement with these measured values. For $\Delta T = 0.007$ K, we obtain $\rho_{liq} = 486.56$ Kg m^{-3}, $\rho_{vap} = 439.687$ Kg m^{-3}, $\sigma = 1.16\times10^{-7}$ n m^{-1}, $\eta_{liq} = 4.07\times10^{-5}$ Pa s and $\eta_{vap} = 3.68\times10^{-5}$ Pa s. At this temperature we are not aware of experimentally measured values of σ, η_{liq} or η_{vap}.

Both the FHS and the model show the saturation of the selected wavelength at higher frequencies (figure 4*a*). For $\Delta T = 0.078$ K, the critical wavelengths λ_c predicted by the FHS and by the model both agree well with experiment, except at low frequencies. For $\Delta T = 0.007$ K, the dispersion curve predicted by the FHS agrees much better with experiment than that predicted by the model. However, the stability thresholds of figure 4(*b*), like those of figure 3, reveal the most significant shortcoming in the model: a_c predicted by the model disagrees significantly with the experimental results, and cannot be improved by varying $\rho_{liq}+\rho_{vap}$, σ and η_{liq}.

These trends persist for other values of ΔT (not shown in the figure 4*a*). For all $\Delta T \geqslant 0.078$ K, by varying $\rho_{liq}+\rho_{vap}$, σ and η_{liq} the critical wavelength and stability threshold obtained by the FHS can be fit to the experimental data reasonably well, except at low excitation frequencies. In contrast, for smaller ΔT (e.g. $\Delta T = 0.007$ K), the prediction by the FHS for λ_c remains below the experimental results for the entire range of excitation frequency. Varying all parameters, i.e. $\rho_{liq}+\rho_{vap}$, σ and η_{liq} by reasonable amounts does not improve the agreement with experimental results.

We can propose various sources for the discrepancy between the experimental data and the results of the FHS for λ_c. Meniscus waves, the no-slip condition at the lateral walls, liquid–vapour mixing and compressibility of the fluids may all affect the wavelength selection. A detailed discussion on various damping mechanisms in a fully confined fluid at temperatures far from the L–V critical point is given by Miles (1967). Because the surface tension decreases rapidly close to the L–V point, the effect of meniscus waves is expected to be small. Since the size of the viscous boundary layer is proportional to $(\nu/\omega)^{1/2}$, the effect of sidewalls, for a given viscosity, is greater at low excitation frequency. This may explain the disagreement of the prediction of the FHS with the experimental values of λ_c at low frequencies for $\Delta T = 0.078$ K. For smaller ΔT, the liquid–vapour mixing and the effects due to compressibility might not be negligible. This might be the reason why varying all parameters does not give better agreement between the prediction of the FHS and the experimental results at $\Delta T =$ 0.007 K.

Based on our observations, we propose a method for measuring the densities and dynamic viscosities of two phases, and the surface tension of the interface in a liquid–vapour system. Any liquid–vapour system can be parametrically excited under vertical oscillation and the critical wavelength λ_c and the threshold a_c measured experimentally over a wide range of excitation frequencies. If the density difference $(\rho_{liq}-\rho_{vap})$, critical density ρ_c and critical temperature T_c are known by other experiments or by theory, we fit the experimental results by varying three parameters: the sum $(\rho_{liq}+\rho_{vap})$, the surface tension σ and η_{liq} (or η_{vap}, since we assume $\nu_{liq} \approx \nu_{vap}$). In principle this gives all the quantities ρ_{liq}, ρ_{vap}, η_{liq} and σ. We note that the dispersion relation is more sensitive to σ and the stability threshold to the dynamic viscosity, facilitating the fitting procedure. This technique should work for temperature differences for which liquid–vapour mixing and/or compressibility effects are less important.

6. Conclusions

We have presented a linear stability analysis for the interface of two viscous fluids using Floquet theory. The effect of large viscosity on the wavelength selection is substantial. We have also presented a simple model and compared its results with the full hydrodynamic system. The prediction of the stability threshold by the FHS agrees very well with that of the experimental results, while the model is unable to predict the stability threshold accurately even at small viscosities. As the viscous stress at the interface increases with viscosity, the critical mode is expected to be distorted significantly at large viscosity. Therefore, consideration of viscous boundary conditions is necessary, not only for obtaining a quantitatively better estimate of the stability threshold, but also for understanding the underlying mechanisms of pattern selection in any weakly nonlinear theory for viscous fluids. Based on the theory, we have proposed a simple technique for measuring the sum of the densities and the dynamic viscosities of liquid–vapour phases of a fluid, and the surface tension coefficient of its interface. We have also generalized the stability problem (Appendix A) to consider a multi-layer system of heterogeneous fluids under parametric excitation.

We have benefited greatly from stimulating discussions with S. Fauve, W. S. Edwards, H. W. Müller and C. Laroche. Experimental data for figure 3 were provided to us by W. S. Edwards. This work has been supported by the CNES (Centre National d'Etudes Spatiales) under Contracts Nos 91/277 and 92/0328. One of us (L.S.T.) was supported by the Fondation Scientifique of the Région Rhône-Alpes.

Appendix A. Stability of a multilayer system of heterogeneous fluids under parametric oscillation

We consider an arrangement in which many layers of incompressible fluids of variable density and dynamic viscosity are superposed and confined between two horizontal plates subjected to a vertical sinusoidal oscillation. The pressure P, density ρ and dynamic viscosity η are assumed to be functions of the vertical coordinate z. The basic state is stationary with all interfaces flat. An interface located at $z = z_s$ ($s = 1, 2, 3, \cdots$), where the density and the viscosity are discontinuous, is subjected to forces due to surface tension σ_s in the presence of any perturbation. Following Chandrasekhar (1970, §91), the linearized equations for perturbations $(u_l, p, \delta\rho)$ for such a system, in a frame of reference fixed to the vibrating plates, can be written as

$$\rho\,\partial_t u_l = -\partial_l p + \eta\nabla^2 u_l + (\partial_l w + \partial_z u_l)(\partial_z \eta) - e_l[G(t)(\delta\rho) - \sum_s (\sigma_s \nabla_H^2 \zeta_s)\,\delta(z - z_s)], \quad \text{(A 1)}$$

$$\partial_l u_l = 0, \quad \text{(A 2)}$$

$$\partial_t(\delta\rho) = -w(\partial_z \rho) \Rightarrow \delta\rho = -(\partial_z \rho)\int w\,\mathrm{d}t, \quad \text{(A 3)}$$

$$\partial_t \zeta_s = w_s \Rightarrow \zeta_s = \int w_s\,\mathrm{d}t. \quad \text{(A 4)}$$

In the above $G(t) = g - a\cos(\omega t)$, $\boldsymbol{e} = (001)$, $w(= u_l e_l)$ is the vertical velocity and ζ_s the deviation of the sth interface from its preassigned value z_s. Equation (A 3) states the incompressibility condition (i.e. $\mathrm{D}_t \rho(z) = 0$, where D_t is the material derivative) for a fluid of variable density. The constant of integration in (A 3) is zero because the interfaces remain flat and stationary with respect to the moving frame in the absence of any velocity perturbation. Similarly the constant of integration in (A 4) is zero because the density $\rho(z)$ at any point remains unchanged if there is no fluid motion.

The boundary conditions at interfaces of viscous fluids demand continuity across every interface of all velocity components and of tangential components of the viscous stress. Making use of (A 2), these conditions at $z = z_s$ can be expressed as

$$\Delta_s w = 0 \quad \text{(continuity of } w\text{)}, \tag{A 5}$$

$$\Delta_s \partial_z w = 0 \quad \text{(continuity of } \partial_z w\text{)}, \tag{A 6}$$

$$\Delta_s \eta(\partial_{zz} - \nabla_H^2) w = 0 \quad \text{(continuity of tangential stress)}. \tag{A 7}$$

Condition (A 7) implies that $\partial_{zz} w$ is finite at an interface. Here, $\Delta_s \chi \equiv \chi|_{z=\zeta_s+} - \chi|_{z=\zeta_s-}$ is the jump in quantity χ at $z = z_s$ and applies to all terms appearing to its right.

Taking the horizontal divergence of (A 1) and using (A 2) we arrive at

$$\nabla_H^2 p = (\rho \partial_t - \eta \nabla^2) \partial_z w - (\partial_z \eta)(\partial_{zz} - \nabla_H^2) w. \tag{A 8}$$

Using (A 3) in the z-component of (A 1) we obtain

$$\partial_z p = -\rho \partial_t w + \eta \nabla^2 w + 2(\partial_z \eta)(\partial_z w) + G(t)(\partial_z \rho) \int w \, dt + (\sigma_s \nabla_H^2 \zeta_s) \delta(z - z_s). \tag{A 9}$$

To interpret (A 9) correctly we must integrate it across the interface. Using (A 5) and (A 6) and the boundedness of $\partial_{zz} w$, (A 9) can be integrated over an infinitesimal length element dz including z_s. Using (A 4), the result can be written as

$$\Delta_s p = 2(\partial_z w)_s \Delta_s \eta + G(t) \zeta_s \Delta_s \rho + \sigma_s \nabla_H^2 \zeta_s. \tag{A 10}$$

In the above the subscript s denotes the value of any quantity which is continuous across an interface, at the sth interface. Another expression for the jump in pressure p across the sth interface, from (A 8), is

$$\Delta_s \nabla_H^2 p = \Delta_s[(\rho \partial_t - \eta \nabla^2) \partial_z w - (\partial_z \eta)(\partial_{zz} - \nabla_H^2) w]. \tag{A 11}$$

Eliminating p from (A 10) and (A 11) we arrive at the jump condition

$$\Delta_s[(\rho \partial_t - \eta \nabla^2) \partial_z w - (\partial_z \eta)(\partial_{zz} - \nabla_H^2) w] = 2\nabla_H^2 (\partial_z w)_s \Delta_s \eta + G(t) \nabla_H^2 \zeta_s \Delta_s \rho + \sigma_s \nabla_H^4 \zeta_s. \tag{A 12}$$

This equation can be viewed as an additional boundary condition at the surface. Equations (A 1)–(A 7) and (A 12) along with a given density and viscosity profile and appropriate boundary conditions at the top and the bottom plates constitute the complete stability problem. For fluids completely enclosed in a vessel, the boundary conditions at the lateral walls must also be specified.

In the absence of external excitation, our system reduces to the problem of Rayleigh–Taylor instability for viscous fluids (Chandrasekhar 1970, §91). For two fluids of different but constant densities and viscosities extending infinitely in the horizontal plane this system gives the set of equations obtained in §2.2. For one fluid of varying density $\rho(z)$, these equations describe internal gravity waves under parametric excitation.

Appendix B. Boundary conditions for the Full Hydrodynamic System

In the Floquet expansions (3.1) and (3.2), the nth coefficient w_{jn} of the vertical velocity in the jth fluid layer is given by (3.7): $w_{jn}(z) = a_{jn} e^{kz} + b_{jn} e^{-kz} + c_{jn} e^{q_{jn} z} + d_{jn} e^{-q_{jn} z}$. The eight coefficients in (3.7) are expressed in terms of the nth coefficient ζ_n of the interface position by means of the eight equations (2.27) and (2.19)–(2.25), written as follows.

Kinematic condition:

$$a_{1n}+b_{1n}+c_{1n}+d_{1n}=[\mu+\mathrm{i}(\alpha+n\omega)]\,\zeta_n. \tag{B 1}$$

Continuity conditions at the interface:

$$a_{1n}+b_{1n}+c_{1n}+d_{1n}=a_{2n}+b_{2n}+c_{2n}+d_{2n}, \tag{B 2}$$

$$k(a_{1n}-b_{1n})+q_{1n}(c_{1n}-d_{1n})=k(a_{2n}-b_{2n})+q_{2n}(c_{2n}-d_{2n}), \tag{B 3}$$

$$\eta_1[2k^2(a_{1n}+b_{1n})+(q_{1n}^2+k^2)(c_{1n}+d_{1n})]=\eta_2[2k^2(a_{2n}+b_{2n})+(q_{2n}^2+k^2)(c_{2n}+d_{2n})]. \tag{B 4}$$

Finite lower layer:

$$a_{1n}\,\mathrm{e}^{-kh_1}+b_{1n}\,\mathrm{e}^{kh_1}+c_{1n}\,\mathrm{e}^{-q_{1n}h_1}+d_{1n}\,\mathrm{e}^{q_{1n}h_1}=0, \tag{B 5}$$

$$k(a_{1n}\,\mathrm{e}^{-kh_1}-b_{1n}\,\mathrm{e}^{kh_1})+q_{1n}(c_{1n}\,\mathrm{e}^{-q_{1n}h_1}-d_{1n}\,\mathrm{e}^{q_{1n}h_1})=0. \tag{B 6}$$

Infinite lower layer:

$$b_{1n}=0, \quad d_{1n}=0. \tag{B 7), (B 8}$$

Finite upper layer:

$$a_{2n}\,\mathrm{e}^{kh_2}+b_{2n}\,\mathrm{e}^{-kh_2}+c_{2n}\,\mathrm{e}^{q_{2n}h_2}+d_{2n}\,\mathrm{e}^{-q_{2n}h_2}=0, \tag{B 9}$$

$$k(a_{2n}\,\mathrm{e}^{kh_2}-b_{2n}\,\mathrm{e}^{-kh_2})+q_{2n}(c_{2n}\,\mathrm{e}^{q_{2n}h_2}-d_{2n}\,\mathrm{e}^{-q_{2n}h_2})=0. \tag{B 10}$$

Infinite upper layer:

$$a_{2n}=0, \quad c_{2n}=0. \tag{B 11), (B 12}$$

REFERENCES

BENJAMIN, T. B. & SCOTT, J. C. 1979 Gravity–capillary waves with edge constraints. *J. Fluid Mech.* **92**, 241–267.

BENJAMIN, T. B. & URSELL, F. 1954 The stability of a plane free surface of a liquid in vertical periodic motion. *Proc. R. Soc. Lond.* A **225**, 505–515.

CHANDRASEKHAR, S. 1970 *Hydrodynamic and Hydromagnetic Stability*, 3rd edn. Clarendon.

CILIBERTO, S., DOUADY, S. & FAUVE, S. 1991 Investigating space-time chaos in Faraday instability by means of the fluctuations of the driving acceleration. *Europhys. Lett.* **15**, 23–28.

CILIBERTO, S. & GOLLUB, J. P. 1985 Phenomenological model of chaotic mode competition in surface waves. *Nuovo Cimento* **6D**, 309–316.

DOUADY, S. 1990 Experimental study of the Faraday instability. *J. Fluid Mech.* **221**, 383–409.

EDWARDS, W. S. & FAUVE, S. 1992 Structure quasicrystalline engendrée par instabilité parametrique. *C. R. Acad. Sci. Paris* **315**, 417–420.

EDWARDS, W. S. & FAUVE, S. 1993 Parametrically excited quasicrystalline surface waves. *Phys. Rev.* E **47**, R788–791.

EZERSKII, A. B., KOROTIN, P. I. & RABINOVICH, M. I. 1985 Random self-modulation of two dimensional structures on a liquid surface during parametric excitation. *Zh. Eksp. theor. Fiz.* **41**, 129–131 (transl. *Sov. Phys. JETP Lett.* **41**, 157–160, 1986).

FARADAY, M. 1831 On the forms and states of fluids on vibrating elastic surfaces. *Phil. Trans. R. Soc. Lond.* **52**, 319–340.

FAUVE, S., KUMAR, K., LAROCHE, C., BEYSENS, D. & GARRABOS, Y. 1992 Parametric instability of a liquid–vapour interface close to the critical point. *Phys. Rev. Lett.* **68**, 3160–3163.

HERPIN, J. C. & MEUNIER, J. 1974 Étude spectrale de la lumière diffusée par les fluctuations thermiques de l'interface liquid vapeur de CO_2 près de son point critique: mesure de la tension superficielle et de la viscosité. *J. Phys. Paris.* **35**, 847–859.

LAMB, H. 1932 *Hydrodynamics*, 6th edn. Cambridge University Press.

LANDAU, L. D. & LIFSHITZ, E. M. 1987 *Fluid Mechanics*, 2nd edn. Pergamon.

MILES, J. W. 1967 Surface-wave damping in closed basins. *Proc. R. Soc. Lond.* A **297**, 459–475.

MILES, J. W. & HENDERSON, D. 1990 Parametrically forced surface waves. *Ann. Rev. Fluid Mech.* **22**, 143–165.

MOLDOVER, M. R. 1985 Interfacial tension of fluids near critical points and two-scale-factor universality. *Phys. Rev.* A **341**, 1022–1033.

TUFILLARO, N., RAMASHANKAR, R. & GOLLUB, J. P. 1989 Order–disorder transition in capillary ripples. *Phys. Rev. Lett.* **62**, 422–425.